10 afforded the α,β-unsaturated ester **8** as the key synthetic intermediate.

Before attempting the formation of the main skeleton of **1** from **8** by the IMDA reaction, we investigated the computer-aided prediction of the preferable stereoselectivity through theoretical calculations of the stability of the transition structures[14,15] using a simplified model compound **8M**, in which the TBSO group of **8** was replaced with a MeO group (Scheme 3).

Scheme 3. Predicted Preference of Diastereoselectivity in the IMDA Reaction of the Model Compound 8M Based on DFT Calculations

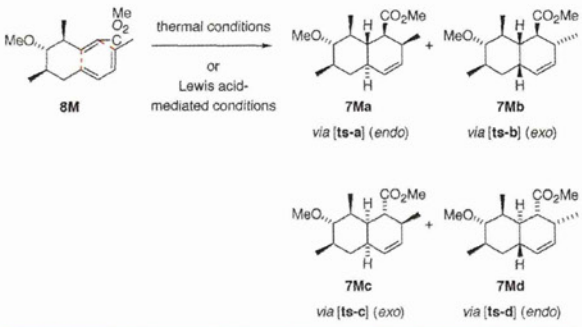

DFT calculations were performed to determine the transition structures that form the fused bicyclic backbone of the multi-substituted 3,4,4a,5,6,7,8,8a-octahydronaphthalene ($\Delta^{1,2}$-octalin). The geometries of all the stationary points were fully optimized at the B3LYP/6-31G* level of theory, and the properties of the molecules were also calculated at the same or advanced level using 6-31G**, 6-311G*, and 6-311G** basis functions. All points were characterized as minima or saddle points by calculation of the harmonic vibrational frequencies using analytical second derivatives.[16]

Four transition states provide the [4 + 2] cycloadducts **7Ma–d**, and these transition structures ([**ts-a1**]–[**ts-d1**]) are categorized as *endo*- and *exo*-modes (*endo*, [**ts-a1**] and [**ts-d1**]; *exo*, [**ts-b1**] and [**ts-c1**]) as depicted in Scheme 4 and Figure 2.

Scheme 4. Transition Structures of the Thermal IMDA Reaction of 8M

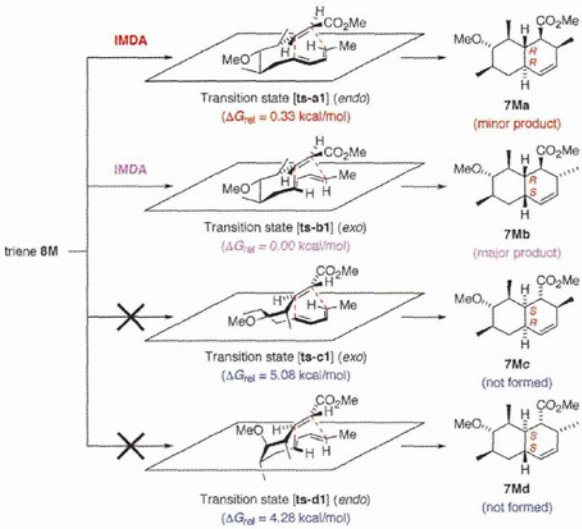

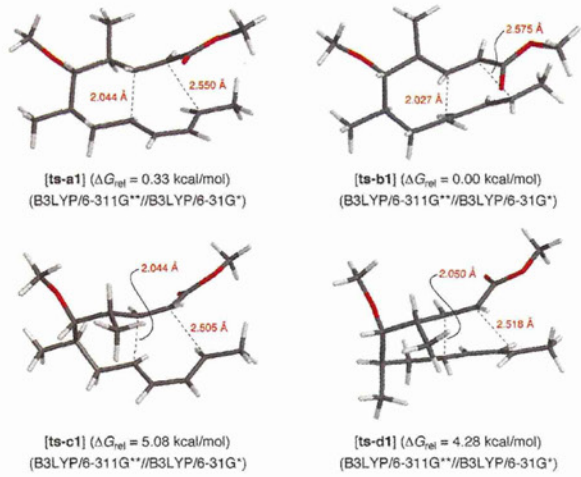

Figure 2. Three-dimensional transition structures, [**ts-a1**] (*endo*), [**ts-b1**] (*exo*), [**ts-c1**] (*exo*), and [**ts-d1**] (*endo*), in the thermal IMDA reaction of **8M**.

Table 1. Calculated Relative Gibbs Free Energies (ΔG_{rel}) (in kcal/mol) of the Transition Structures in the Thermal IMDA Reaction of 8M

	B3LYP/ 6-31G*	B3LYP/ 6-31G**	B3LYP/ 6-311G*	B3LYP/ 6-311G**	predict (110 °C)	
[**ts-a1**]	0.49 (0.40)[a]	0.50	0.19 (0.14)[a]	0.33	37	45
					..	..
[**ts-b1**]	0.00 (0.00)[a]	0.00	0.00 (0.00)[a]	0.00	63	55
					.. ~	..
[**ts-c1**]	5.21 (5.12)[a]	5.19	5.26 (5.23)[a]	5.08	0	0
					..	..
[**ts-d1**]	4.65 (4.64)[a]	4.62	4.39 (4.48)[a]	4.28	0	0

[a]The values in parentheses are ΔG_{rel} values at 383.15 K (110 °C).

Scheme 5. Thermal or Et_2AlCl-Mediated IMDA Reaction of 8 to Form *endo*-Type (9*R*,10*R*)-$\Delta^{1,2}$-Octalin 20a via 7a and *exo*-Type (9*S*,10*R*)-$\Delta^{1,2}$-Octalin 20b via 7b[a]

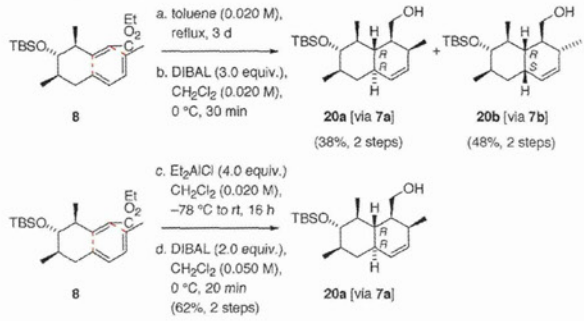

[a]Reagents and conditions: (a) toluene, reflux, 3 d; (b) DIBAL, CH_2Cl_2, 0 °C, 30 min, 38% of **20a** and 48% of **20b** from **8**; (c) Et_2AlCl, CH_2Cl_2, −78 °C to rt, 16 h; (d) DIBAL, CH_2Cl_2, 0 °C, 20 min, 62% of **20a** from **8**.

The desired (9*R*,10*R*)-$\Delta^{1,2}$-octalin derivative **7Ma** could be generated via the transition state [**ts-a1**] by the IMDA reaction of the model triene **8M**. Another *endo*-mode transition state [**ts-d1**] to form the diastereoisomeric (9*S*,10*S*)-$\Delta^{1,2}$-octalin derivative **7Md** is an unfavorable structure for the preparation of **1**. Similarly, the *exo*-mode transition states, [**ts-b1**] and [**ts-c1**], could be converted into the undesired (9*S*,10*R*)- and (9*R*,10*S*)-$\Delta^{1,2}$-octalin

dx.doi.org/10.1021/jm301695c | J. Med. Chem. 2013, 56, 150–159

Scheme 6. Transition Structures of the Me_2AlCl-Mediated IMDA Reaction of 8M

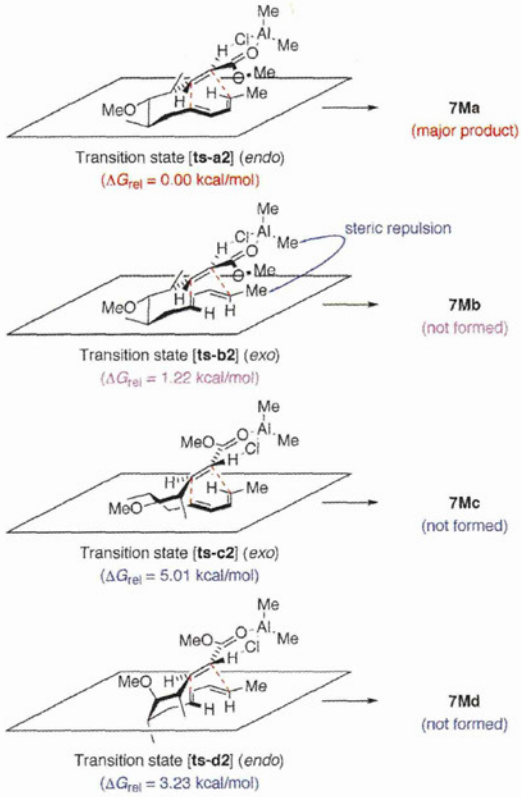

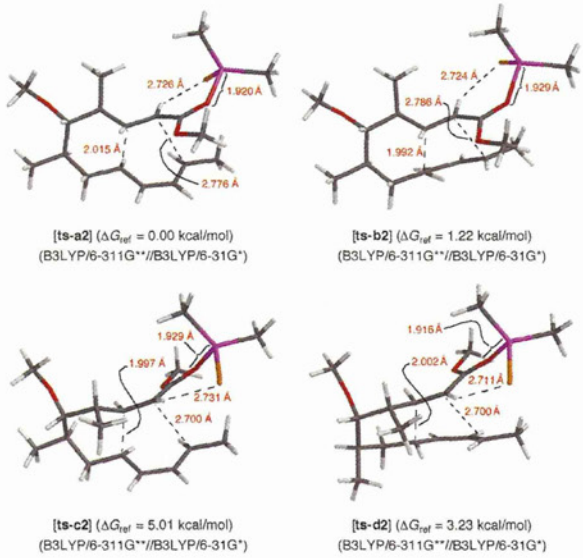

Figure 3. Three-dimensional transition structures, [**ts-a2**] (*endo*), [**ts-b2**] (*exo*), [**ts-c2**] (*exo*), and [**ts-d2**] (*endo*), in the Me_2AlCl-mediated IMDA reaction of **8M**.

derivatives **7Mb** and **7Mc** through the imaginary IMDA reactions, respectively. The calculated relative Gibbs free energy (ΔG_{rel}) is shown under each transition structure in Scheme 4 and Table 1. It was revealed that [**ts-c1**] and [**ts-d1**] have significantly high ΔG_{rel} values compared with those of [**ts-a1**] and [**ts-b1**] because of the steric repulsion between the methyl group at the C-4 position in **8M** and the surroundings in these transition structures. Therefore, the corresponding (9*R*,10*S*)- and (9*S*,10*S*)-$\Delta^{1,2}$-octalin derivatives **7Mc** and **7Md** will hardly form via these two highly strained transition states (ΔG_{rel} = 5.21−5.08 kcal/mol for [**ts-c1**]; ΔG_{rel} = 4.65−4.28 kcal/mol for [**ts-d1**]). Within the stable [**ts-a1**] and [**ts-b1**] structures having lower values of ΔG_{rel}, the formation of the latter transition structure is preferable. The calculated free-energy

Table 2. Calculated Relative Gibbs Free Energies (ΔG_{rel}) (in kcal/mol) of the Transition Structures in the Me_2AlCl-Mediated IMDA Reaction of 8M

	B3LYP/ 6-31G*	B3LYP/ 6-31G**	B3LYP/ 6-311G*	B3LYP/ 6-311G**	predict (25 °C)
[**ts-a2**]	0.00	0.00	0.00	0.00	93 .. 89
[**ts-b2**]	1.50	1.41	1.32	1.22	7 .. ∼ .. 11
[**ts-c2**]	5.33	5.27	5.23	5.01	0 .. 0
[**ts-d2**]	3.48	3.34	3.51	3.23	0 0

Scheme 7. Completion of Total Syntheses of 1 and 2[a]

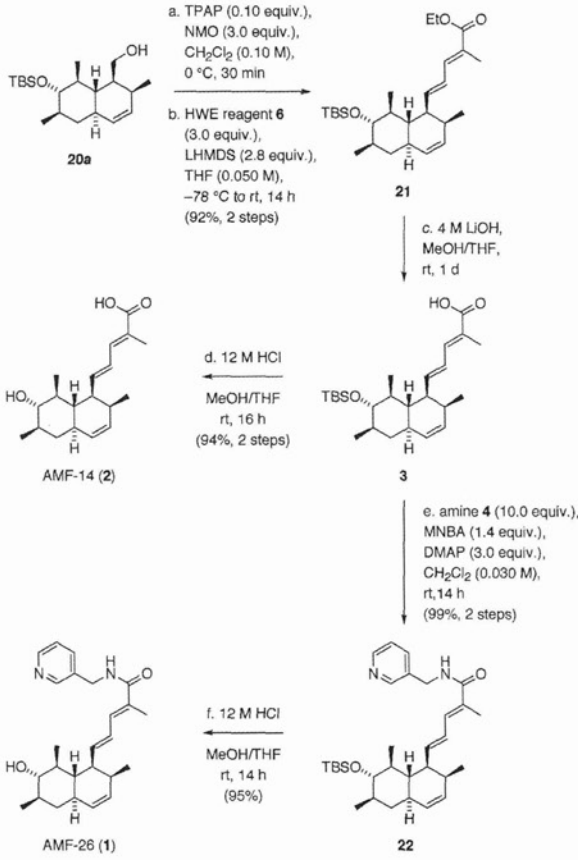

[a]Reagents and conditions: (a) TPAP, NMO, CH_2Cl_2, 0 °C, 30 min; (b) phosphate **6**, LHMDS, THF, −78 °C to rt, 14 h, 92% from **20a**; (c) 4 M LiOH, MeOH, THF, rt, 1 d; (d) 12 M HCl, MeOH, THF, rt, 16 h, 94% from **21**; (e) amine **4**, MNBA, DMAP, CH_2Cl_2, rt, 14 h, 99% from **21**; (f) 12 M HCl, MeOH, THF, rt, 14 h, 95%.

dx.doi.org/10.1021/jm301695c | J. Med. Chem. 2013, 56, 150−159

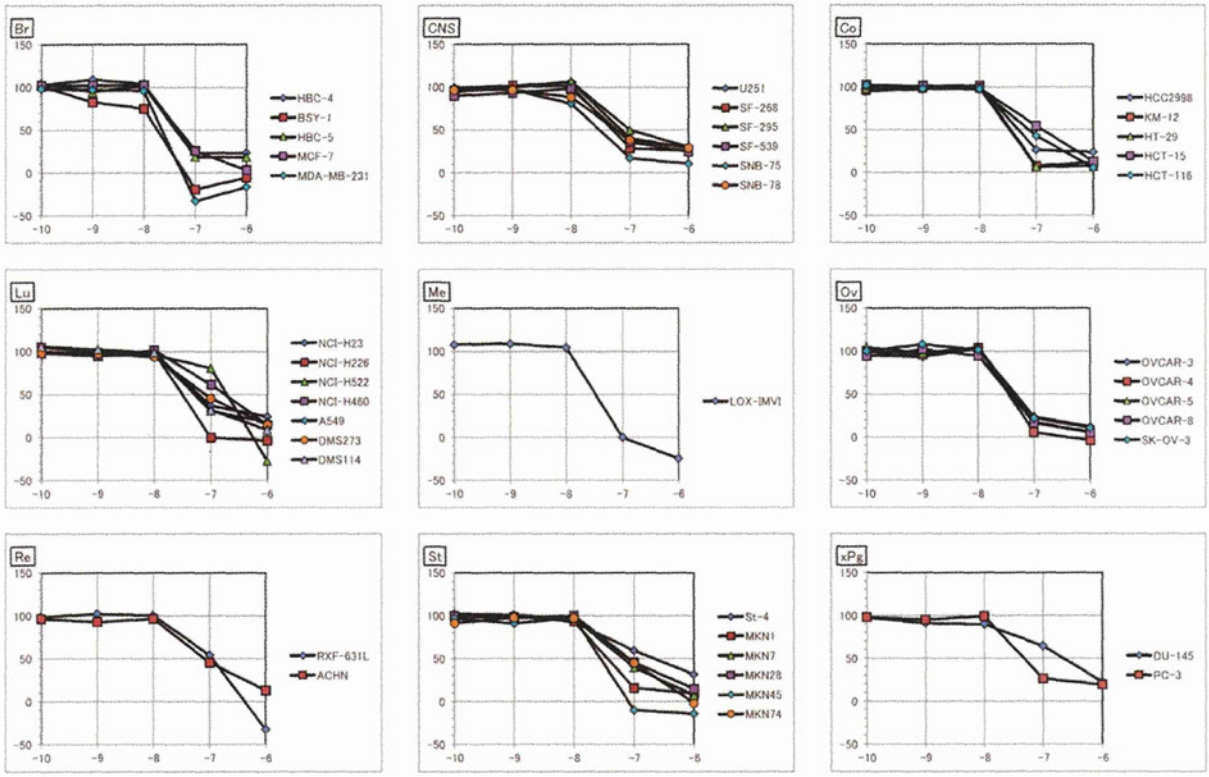

Figure 4. Growth inhibition against a panel of human cancer cell lines. Dose-dependent effects of the totally synthetic **1** on each cancer cell were measured as described in the experimental procedures. The *x*-axis represents the logarithm of the mean of the GI50 values (log[concentration (M)]) for each cell line. The *y*-axis represents the growth rate of each human cancer cell line (% of control). Quantification of the GI50 value was represented as the mean of four different experiments. Br, breast; CNS, central nervous system; Co, colon; Lu, lung; Me, melanoma; Ov, ovary; Re, renal; St, stomach; xPg, prostate.

difference (ΔG_{rel} = 0.49–0.19 kcal/mol at 298.15 K (25 °C); 0.40–0.14 kcal/mol at 383.15 K (110 °C)) corresponds to the medium diastereomeric ratio of the formed [4 + 2] cycloadducts according to the Boltzmann distribution (estimated selectivity of **7Ma**:**7Mb** = ~30:70–42:58 at 298.15 K (25 °C); ~37:63–45:55 at 383.15 K (110 °C)).

Thermal IMDA Reaction of 8 to Form $\Delta^{1,2}$-Octalins 20a and 20b and Et_2AlCl-Mediated Diastereoselective IMDA Reaction of 8 to Form $\Delta^{1,2}$-Octalin 20a. After determining the transition structures and understanding the nature of the predictable stereoselectivity of the IMDA reaction of **8M**, we eventually examined the thermal transformation of **8**, which has a TBSO group at the C-5 position instead of a MeO group at the same position in **8M**. By heating **8** in toluene at reflux temperature for three days (Scheme 5, upper equation), the desired thermal [4 + 2] cycloaddition reaction successfully proceeded, and we obtained a mixture of two stereoisomeric products, **7a** and **7b**, corresponding to the model $\Delta^{1,2}$-octalins **7Ma** and **7Mb**, respectively. A mixture of the cycloadducts, **7a** and **7b**, was then treated with DIBAL to provide the desired primary alcohols, **20a** and **20b**, with a low diastereoselectivity (**20a**:**20b** = ~44:56) in this two-step transformation. These experimental results are in good agreement with the assumed stereoselectivity as follows: (1) Two products, **7a** and **7b**, possessing (*R*) configurations at the C-10 position were predominantly produced, and two other $\Delta^{1,2}$-octalins possessing (*S*) configurations at the same position were not obtained at all. (2) Both the major stereoisomer, (9*S*,10*R*)-**7b**, generated from the *exo*-mode transition state, and the minor one, (9*R*,10*R*)-**7a**, generated from the *endo*-mode transition state, were simultaneously produced because the predicted preference of the *exo*-mode transition state over the *endo*-mode transition state is not very high.

To improve the yield of the *endo*-type (9*R*,10*R*)-$\Delta^{1,2}$-octalin derivative **7a**, a favorable intermediate for the synthesis of **1**, it is necessary to develop an alternative activation method for the IMDA reaction that proceeds via the *endo*-mode transition state [**ts-a1**] but not via the *exo*-mode transition state [**ts-b1**]. There are many successful examples of obtaining *endo*-type octalin derivatives via the diastereoselective Diels–Alder reaction using a Lewis acid in steroid syntheses;[17] therefore, we decided to use the Et_2AlCl-mediated Diels–Alder reaction to control the diastereoselectivity of the IMDA reaction of **8**.

Determination of the structures of the *endo*- and *exo*-mode transition states with Me_2AlCl and the relative Gibbs free energies was next carried out by theoretical calculations according to the above-mentioned method for predicting the diastereoselectivity that uses the model substrate **8M**. The optimized *endo*-mode transition structures [**ts-a2**] and [**ts-d2**], and *exo*-mode transition structures [**ts-b2**] and [**ts-c2**] are described in Scheme 6 and Figure 3, in which all ester-carbonyl groups are activated by Me_2AlCl. Each chloride atom in [**ts-a2**]–[**ts-d2**] locates near an α-proton of the ester group because a hydrogen-bonding interaction occurs between the electronically negative chloride atom and electronically positive hydrogen atom. Therefore, stable

dx.doi.org/10.1021/jm301695c | J. Med. Chem. 2013, 56, 150–159

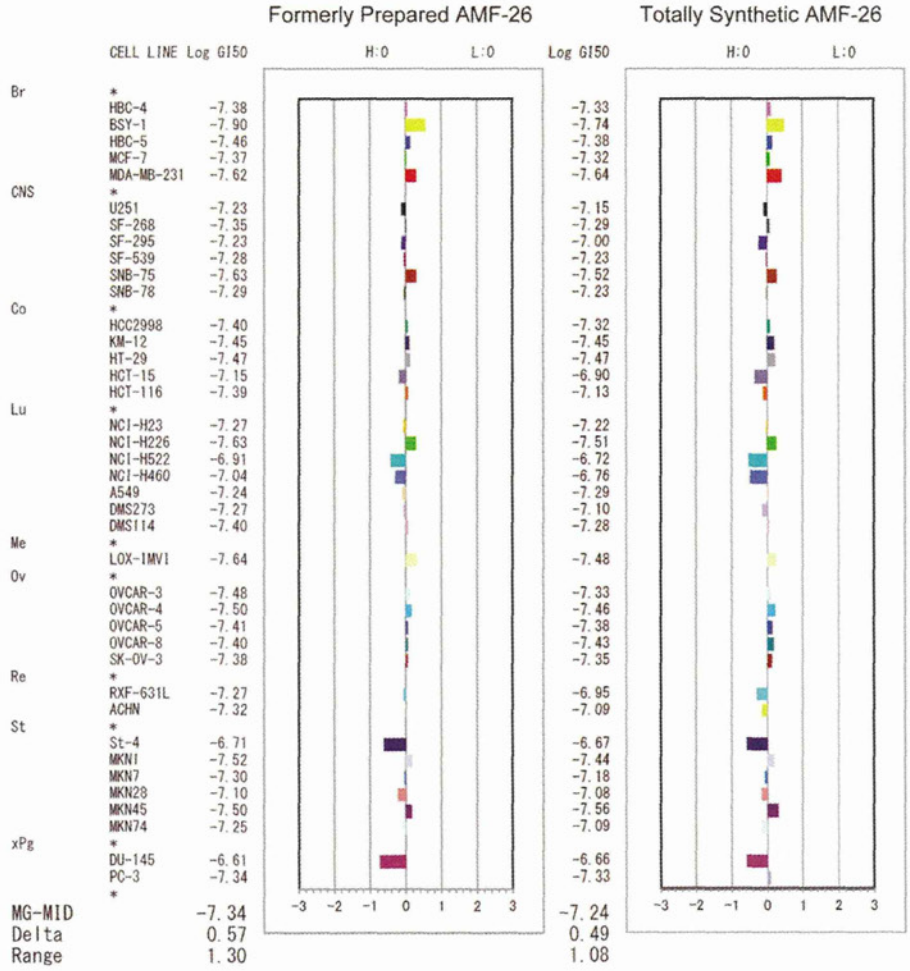

Figure 5. Fingerprints of the formerly prepared **1** and totally synthetic **1**. Growth inhibition was assessed against a panel of 39 human cancer cell lines. Fingerprints were produced by computer processing of the 50% growth inhibition (GI50) values. The logarithm of the GI50 value for each cell line is indicated in the figure. In the plot, columns to the right of zero indicate the sensitivity of the cell line to the compound, and columns to the left indicate resistance to the compound. The *x*-axis represents the logarithm of the difference between the mean of the GI50 values for 39 cell lines and the GI50 value for each cell line in the JFCR39 panel. The fingerprint of the totally synthetic **1** (right column) significantly correlated with that of the formerly prepared **1** derived from a natural molecule **2** (left column) (Pearson correlation coefficient $r = 0.843$). MG-MID, the mean of the log GI50 values for the 39 cell lines; delta, the logarithm of the difference between the MG-MID and log GI50 of the most sensitive cell line; range, the logarithm of the difference between the log GI50 of the most resistant cell line and log GI50 of the most sensitive cell line. One scale represents one logarithm difference.

six-membered rings, including (i) a strong coordination of the oxygen atoms in ester groups to aluminum atoms and (ii) an additional hydrogen-bonding interaction between the chloride atoms in Me_2AlCl and C-2 protons of the ester groups, were efficiently created in these transition states. However, the calculated relative Gibbs free energies in Table 2 indicate that (i) [**ts-c2**] and [**ts-d2**] have higher ΔG_{rel} values (5.33−5.01 kcal/mol for [**ts-c2**]; 3.51−3.23 kcal/mol for [**ts-d2**]) compared with those of [**ts-a2**] and [**ts-b2**] similar to the thermal IMDA reaction of **8M**, (ii) the *endo*-mode transition state [**ts-a2**] is more stable than the *exo*-mode transition state [**ts-b2**] because the ΔG_{rel} of [**ts-a2**] is much lower than that of [**ts-b2**] (ΔG_{rel} = 1.50−1.22 kcal/mol at 298.15 K (25 °C)). It is assumed that the steric repulsion between one of the methyl groups in Me_2AlCl and the substrate is quite high during the conversion of the triene **8M**−Me_2AlCl complex into the transition structure [**ts-b2**] as depicted in Scheme 6.

On the basis of the present preferable theoretical prediction, we actually examined the IMDA reaction of **8** using Et_2AlCl instead of the ideal reaction of **8M** with Me_2AlCl, and the desired **20a** was solely obtained after reducing the temporarily formed **7a**; namely, the production of the *endo*-type (9*R*,10*R*)-$\Delta^{1,2}$-octalin derivative **7a** exclusively occurs without formation of not only the *exo*-type (9*S*,10*R*)-$\Delta^{1,2}$-octalin derivative **7b** but also other stereoisomers, such as the (9*R*,10*S*)- and (9*S*,10*S*)-$\Delta^{1,2}$-octalin derivatives **7c** and **7d** (Scheme 5, bottom equation).

Completion of the First Total Synthesis. Next, installation of the $\alpha,\beta,\gamma,\delta$-bisunsaturated ester moiety in the (9*R*,10*R*)-$\Delta^{1,2}$-octalin derivative **20a** was attempted, as shown in Scheme 7. Oxidation of **20a** using TPAP with NMO was carried out to provide the corresponding aldehyde **5**, and the following HWE olefination of the resulting aldehyde **5** with phosphate **6**[18] smoothly proceeded to afford the desired triene **21** in good yield. After hydrolysis of the ester moiety in **21** with lithium hydroxide,

dx.doi.org/10.1021/jm301695c | J. Med. Chem. 2013, 56, 150−159

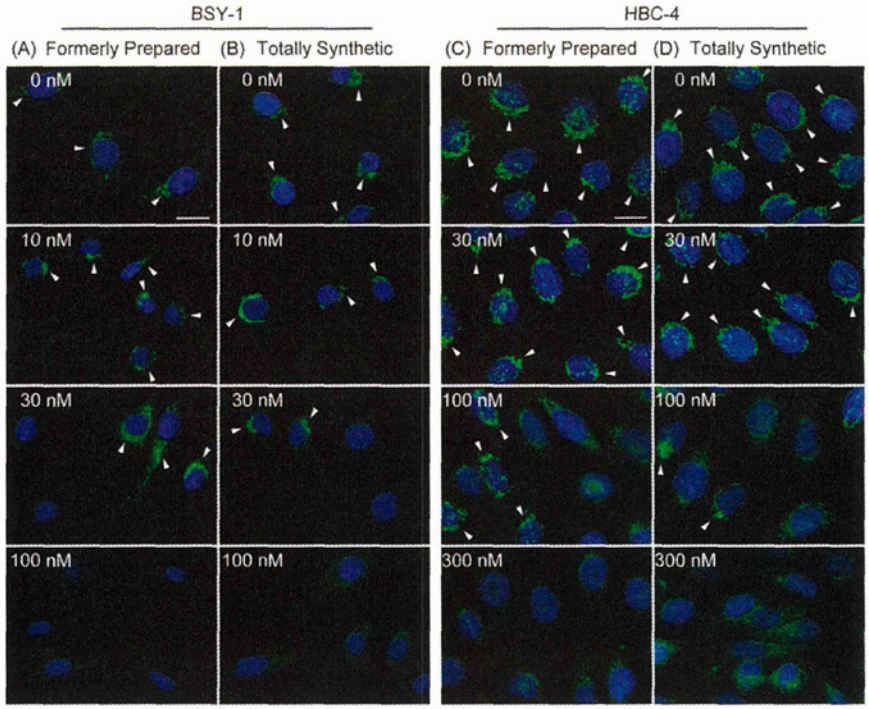

Figure 6. Disrupting Golgi apparatus by the formerly prepared **1** and totally synthetic **1** [dispersion of GBF1 in BSY-1 cells (A and B) or HBC-4 cells (C and D)]. Cells were treated with either the formerly prepared **1** (A and C) or the totally synthetic **1** (B and D) at different concentrations for 1 h. The cells were then fixed and labeled with anti GBF1 (green) and DAPI (blue). In the BSY-1 and HBC-4 cells treated with the formerly prepared **1** or the totally synthetic **1**, GBF1 was dispersed from the perinuclear region, which gave a ribbon-like appearance (white arrowhead), into the cytoplasm. Scale bar: 20 μm.

deprotection of the silyl ether group at the C-6 position of the resulting carboxylic acid **3** was eventually examined using 12 M hydrochloric acid, and the desired product **2** was readily prepared in excellent yield by this facile procedure.[19] All the spectral data, including the optical rotation of the totally synthetic **2**, corresponded to those reported for naturally occurring (+)-**2** (our synthetic sample; $[\alpha]_D^{24}$ +56.4 (*c* 0.593, MeOH), lit[1,2] $[\alpha]_D^{20}$ +58.71 (*c* 0.998, MeOH)), and all the absolute configurations of the stereogenic centers at the C-3, C-4, C-5, C-6, C-7, C-9, and C-10 positions were unequivocally determined by this identification. On the other hand, it was revealed that MNBA-mediated amidation[12] using an excess amount of DMAP (3.0 equiv) in the absence of triethylamine produced the 3-picolylamide **22** from the carboxylic acid **3** in a satisfactory yield. Finally, the transformation of **22** by deprotection of the TBS group furnished the targeted molecule **1** in very high yield.[19] Thus, an efficient method for the synthesis of **1** was established via the Et_2AlCl-mediated diastereoselective IMDA reaction of the chiral linear precursor **8**. The synthesis of **1** proceeds in 14 steps and 19% overall yield from the chiral oxazolidinone **16**. The ^1H and ^{13}C NMR spectra of the obtained **1** showed that the synthetic sample has the same relative stereochemistry as formerly prepared **1** derived from naturally occurring **2**. Other properties of the synthetic **1** including its optical rotation were identical to those of formerly prepared (+)-**1** derived from (+)-**2** (our synthetic sample; $[\alpha]_D^{26}$ +73.6 (*c* 0.480, MeOH), lit[1,2] $[\alpha]_D^{20}$ +76.69 (*c* 1.103, MeOH)).

■ BIOLOGICAL ASSAYS OF THE TOTALLY SYNTHETIC AMF-26

Antitumor Activity of the Totally Synthetic 1 against a Variety of Human Cancer Cell Lines. To obtain a preliminary evaluation of the totally synthetic **1**, we determined the biological activity of the synthetic **1** for cell growth inhibition and disrupting the Golgi system. As shown in Figure 4, the global antitumor activity of the totally synthetic **1** against a variety of human cancer cells was assessed on a panel of 39 human cancer cell lines (JFCR39).[2,20] Among them, the synthetic **1** strongly inhibited the growth of several cancer cell lines at concentrations of less than 0.04 μM (GI50 values at 18.2 nM for BSY-1, 22.9 nM for MDA-MB-231 [breast], 30.2 nM for SNB-75 [central nervous system], 35.5 nM for KM-12, 33.9 nM for HT-29 [colon], 30.9 nM for NCI-H226 [lung], 33.1 nM for LOX-IMVI [melanoma], 34.7 nM for OVCAR-4, 37.2 nM for OVCAR-8 [ovary], and 36.3 nM for MKN1, 27.5 nM for MKN45 [stomach]).

The informatic anticancer drug discovery system, JFCR39, is a powerful tool for extracting compounds with similar modes of action from a database.[20] The JFCR39 panel was coupled with our own drug sensitivity database, which is comparable to that of the NCI60 panel from the National Cancer Institute.[21] By using the COMPARE computer algorithm (details described in the experimental procedures), it is possible to correlate the growth inhibitory patterns of JFCR39 (termed "fingerprints") of a test compound with those of a known compound in the database. We compared the fingerprint of the totally synthetic **1** with that of the formerly prepared **1** derived from a natural molecule **2** (Figure 5) and demonstrated a significant correlation between the two (correlation coefficient $r = 0.843$).

Golgi Disruption and Proliferation Tests of BSY-1 and HBC-4 Cells by the Totally Synthetic AMF-26. We previously reported that **1** disrupted the Golgi system by inhibiting the Arf1 activation.[2] We now examined whether the totally synthetic **1** induced Golgi disassembly by use of immunofluorescence

dx.doi.org/10.1021/jm301695c | J. Med. Chem. 2013, 56, 150−159

staining with a monoclonal antibody to GBF1 (Golgi brefeldin A resistant guanine nucleotide exchange factor 1), a marker of Golgi. In the control cells, GBF1 was observed in the perinuclear region. The addition of the totally synthetic **1** caused a rapid release of GBF1 into the cytoplasm as shown in parts B and D of Figure 6, similar to the addition of the formerly prepared **1** derived from a natural molecule **2**, as shown in parts A and C of Figure 6.

The proliferation of BSY-1 or HBC-4 cells treated with drugs was monitored as shown in Figure 7A. Changes in the amounts of

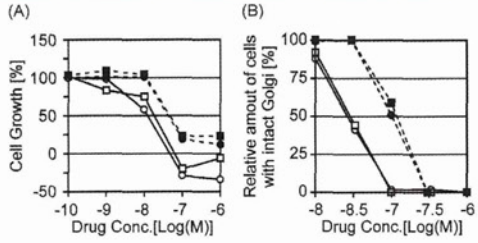

Figure 7. Cell growth inhibition and Golgi disruption by the formerly prepared **1** and totally synthetic **1**. Symbols represent the following: open circle, BSY-1 cells treated with the formerly prepared **1**; open square, BSY-1 cells treated with the totally synthetic **1**; closed circle, HBC-4 cells treated with the formerly prepared **1**; closed square, HBC-4 cells treated with the totally synthetic **1**.

the total cellular protein after 48 h of drug treatment were analyzed using the SRB assay. Furthermore, the BSY-1 or HBC-4 cells were treated with the formerly prepared **1** and totally synthetic **1** at different concentrations for 1 h and then stained with antibodies against GBF1 (Figure 7B). Over 100 features were measured under each condition, and the numbers of cells whose Golgi was dispersed were then counted. The biological efficacy of the totally synthetic **1** was consistent with that of the semisynthesized **1** based on these data; therefore, we concluded that the structure of the totally synthetic **1** was unambiguously identified with that of the formerly prepared **1**, which was derived from a natural compound **2**.

SYNTHESIS AND SAR STUDIES OF AMF-26 DERIVATIVES

By use of intermediate **20a**, we further prepared compounds **26** and **31** as derivatives of **1** as depicted in Schemes 8 and 9, respectively. The two-carbon elongation of the aldehyde derived from **20a** was carried out to afford the corresponding unsaturated ester **23** (Scheme 8). The saponification of **23** and the successive MNBA-mediated amidation of **24** provided **25** in a very high yield. Finally, compound **26**, which includes a shortened side-chain compared to **1**, was successfully obtained by the treatment of **25** with hydrochloric acid. We also prepared another derivative **31** according to the procedure for the synthesis of **1**. As depicted in Scheme 9, compound **31** has a longer alkyl group (ethyl group) at the α-position of the amide group instead of a methyl group at the same position in **1**. We then tried to evaluate the efficacy of these novel derivatives, **26** and **31**, based on SAR studies of the side-chain in **1**. We first determined the biological activity of these derivatives for cell growth inhibition using JFCR39. Figure 1 in the Supporting Information represents fingerprints of the formerly prepared **1**, the totally synthetic **1**, compound **26**, and compound **31**. The experimental conditions and abbreviations are described in Figure 5. The logarithm of the mean GI50 values of compound **31** was −6.11, meaning that the

Scheme 8. Preparation of a Novel Derivative 26[a]

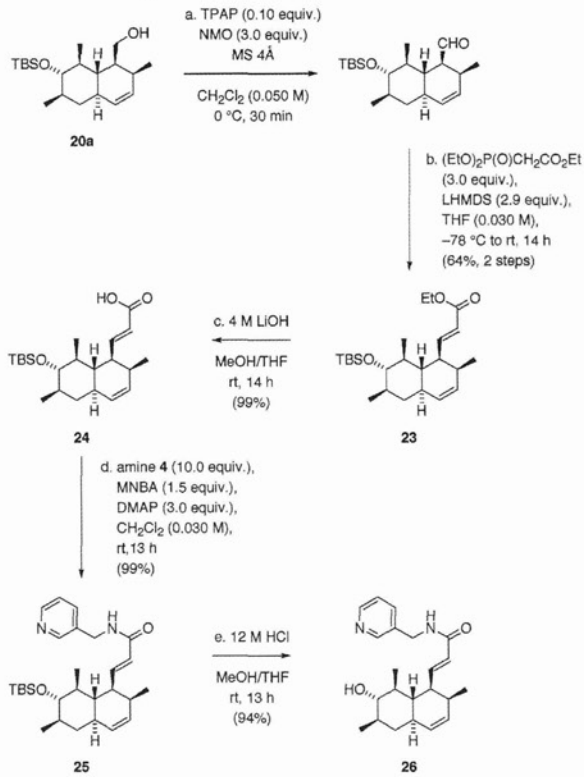

[a]Reagents and conditions: (a) TPAP, NMO, 4-Å molecular sieves, CH_2Cl_2, 0 °C, 30 min; (b) $(EtO)_2P(O)CH_2CO_2Et$, LHMDS, THF, −78 °C to rt, 14 h, 64% from **20a**; (c) 4 M LiOH, MeOH, THF, rt, 14 h, 99%; (d) amine **4**, MNBA, DMAP, CH_2Cl_2, rt, 13 h, 99%; (e) 12 M HCl, MeOH, THF, rt, 13 h, 94%.

growth inhibition efficacy of compound **31** was about 10-fold weaker than that of **1** and its efficacy of the growth inhibition was moderate. The fingerprint of compound **31** significantly correlated that of the formerly prepared **1** (correlation coefficient $r = 0.816$). On the other hand, the logarithm of the mean GI50 values of compound **26** was −4.02, suggesting that this compound showed a very weak efficacy. There was no correlation between the fingerprint of compound **26** and that of the formerly prepared **1** ($r = 0.117$).

Next, we examined the Golgi disruption efficacy of the two derivatives. The addition of compound **31** caused a release of GBF1 into the cytoplasm as depicted in parts B and D of Figure 2 in the Supporting Information. However, no Golgi disruption was observed at the concentration of 1 μM in the compound-**26**-treated BSY-1 cells as depicted in Figure 2A of the Supporting Information or 10 μM in the compound-**26**-treated HBC-4 cells as depicted in Figure 2C of the Supporting Information.

The proliferation of BSY-1 or HBC-4 cells treated with drugs (formerly prepared **1**, the totally synthetic **1**, compound **26**, and compound **31**) was monitored as shown in parts A and B of Figure 3 in the Supporting Information. Furthermore, the observed Golgi disrupting efficacy of all drugs was shown in parts C and D of Figure 3 in the Supporting Information. Modification of the side-chain induced a wide range of biological efficacies. Compound **31** moderately inhibited cell growth (GI50 value at 0.55 μM for HBC-4 and 0.19 μM for BSY-1) and disrupted the Golgi

dx.doi.org/10.1021/jm301695c | J. Med. Chem. 2013, 56, 150−159

Scheme 9. Preparation of a Novel Derivative 31[a]

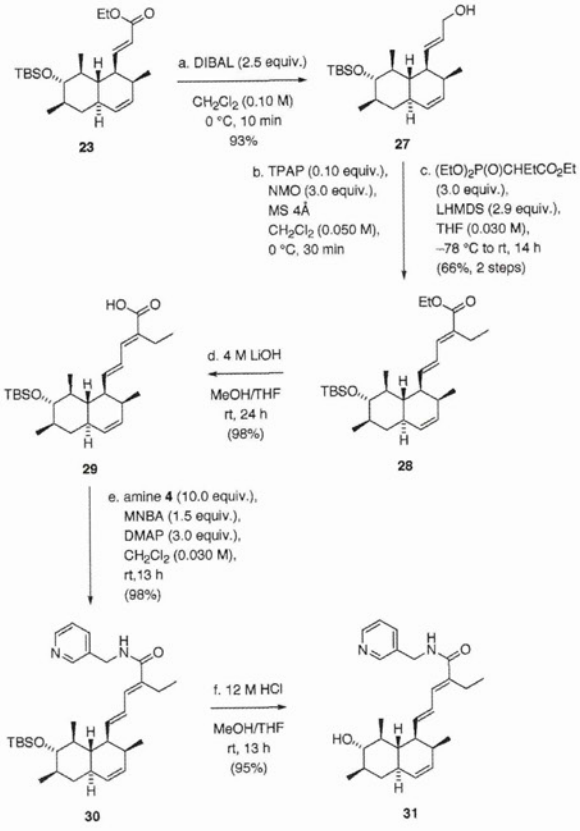

[a]Reagents and conditions: (a) DIBAL, CH_2Cl_2, 0 °C, 10 min, 93%; (b) TPAP, NMO, 4-Å molecular sieves, CH_2Cl_2, 0 °C, 30 min; (c) $(EtO)_2P(O)CHEtCO_2Et$, LHMDS, THF, −78 °C to rt, 14 h, 66% from **27**; (d) 4 M LiOH, MeOH, THF, rt, 24 h, 98%; (e) amine **4**, MNBA, DMAP, CH_2Cl_2, rt, 13 h; 98%; (f) 12 M HCl, MeOH, THF, rt, 13 h, 95%.

apparatus (EC50 value at 0.85 μM for HBC-4 and 0.34 μM for BSY-1); however, compound **26** showed very weak biological activities (both the GI50 value and EC50 value were above 10 μM).[22]

CONCLUSION

In summary, we have developed a convenient method for preparing **1**, a potentially promising new anticancer drug that disrupts the Golgi system by inhibiting the Arf1 activation. We achieved this total synthesis through the stereoselective IMDA reaction of the chiral linear precursor using Et_2AlCl as a Lewis-acid activator. The stereoselectivity of the thermal or Me_2AlCl-mediated IMDA reaction was theoretically presumed by DFT calculations, and the origins of the switching in the reaction modes under these two conditions were plausibly accounted for by a comparison between the relative Gibbs free energies of those transition states in the IMDA reaction. From an assessment of the global antitumor activity of the totally synthetic **1** against a variety of human cancer cells using a panel of 39 human cancer cell lines, it was shown that the synthetic **1** strongly inhibited the growth of several cancer cell lines, such as BSY-1, MDA-MB-231, SNB-75, KM-12, HT-29, NCI-H226, LOX-IMVI, OVCAR-4, OVCAR-8, MKN1, and MKN45, at low concentrations (less than 0.04 μM for GI50). An evaluation of the biological activities of the synthetic **1** in two types of assessments revealed that our synthetic **1** has the same property as the semisynthesized **1** derived from the original natural molecule **2** (correlation coefficient $r = 0.843$). Through both the total synthesis of **1** and identification of the synthetic **1** with the formerly prepared **1** regarding their biological activity, the structure of the formerly prepared **1** has been unequivocally determined. We further synthesized compound **26**, which includes a shortened side-chain compared to **1**, and another derivative **31**, which has a longer alkyl group at the α-position of the amide group instead of a methyl group at the same position in **1**. Compound **26** showed a very weak efficacy, and there was no correlation between the fingerprint of compound **26** and that of **1** ($r = 0.117$). On the other hand, the growth inhibition efficacy of compound **31** was about 10-fold weaker than that of **1** and its fingerprint was significantly correlated to that of **1** ($r = 0.816$). The large-scale production of **1** and its derivatives for the development of novel anticancer drugs are now in progress in this laboratory.

ASSOCIATED CONTENT

Supporting Information

Experimental procedures; supplementary figures for the SAR studies of AMF-26 derivatives **26** and **31**; spectroscopic and analytical data for all new compounds including copies of NMR spectra; Cartesian coordinates of transition states. This material is available free of charge via the Internet at http://pubs.acs.org.

AUTHOR INFORMATION

Corresponding Author

*Phone: +81-3-3260-4271. Fax: +81-3-3260-5609. E-mail: shiina@rs.kagu.tus.ac.jp.

Notes

The authors declare no competing financial interest.

ACKNOWLEDGMENTS

This study was supported by a Health and Labour Sciences Research Grants from the Ministry of Health, Labour and Welfare, Japan.

ABBREVIATIONS USED

ADP, adenosine diphosphate; Arf1, ADP-ribosylation factor 1; IMDA, intramolecular Diels–Alder; JFCR39, a panel of 39 human cancer cell lines in Japanese Foundation for Cancer Research; ArfGEF, guanine nucleotide exchange factor for Arf; VEGF, vascular endothelial growth factor; GBF1, Golgi brefeldin A resistant guanine nucleotide exchange factor 1; DAPI, 4′,6-diamidino-2-phenylindole; KSA, ketene silyl acetal; HWE, Horner–Wadsworth–Emmons; MNBA, 2-methyl-6-nitrobenzoic anhydride; DMAP, 4-(dimethylamino)pyridine; NaHMDS, sodium bis(trimethylsilyl)amide; LHMDS, lithium bis(trimethylsilyl)-amide; TBAI, tetrabutylammonium iodide; TPAP, tetrapropylammonium perruthenate; NMO, 4-methylmorpholine *N*-oxide; TBS, *tert*-butyldimethylsiloxy; DIBAL, diisobutylaluminum hydride; DFT, density functional theory

REFERENCES

(1) Yamada, N. WO2005/070856, 2005, Nippon Shinyaku Co., Ltd.

(2) Ohashi, Y.; Iijima, H.; Yamaotsu, N.; Yamazaki, K.; Sato, S.; Okamura, M.; Sugimoto, K.; Dan, S.; Hirono, S.; Yamori, T. *J. Biol. Chem.* **2012**, *287*, 3885–3897.

(3) Reviews for drug discovery at protein–protein interfaces. (a) Berg, T. *Curr. Opin. Drug Discov. Dev.* **2008**, *11*, 666–674. (b) Wells, J. A.; McClendon, C. L. *Nature* **2007**, *450*, 1001–1009.

(4) Inhibition of Arf1–ArfGEF interaction by brefeldin A: (a) Renault, L.; Guibert, B.; Cherfils, J. *Nature* **2003**, *426*, 525–530. (b) Zeeh, J. C.; Zeghouf, M.; Grauffel, C.; Guibert, B.; Martin, E.; Dejaegere, A.; Cherfils, J. *J. Biol. Chem.* **2006**, *281*, 11805–11814.

(5) Disruption of the Golgi apparatus by brefeldin A: (a) Lippincott-Schwartz, J.; Yuan, L. C.; Bonifacino, J. S.; Klausner, R. D. *Cell* **1989**, *56*, 801–813. (b) Lippincott-Schwartz, J.; Yuan, L.; Tipper, C.; Amherdt, M.; Orci, L.; Klausner, R. D. *Cell* **1991**, *67*, 601–616.

(6) Inhibition of tumor growth by brefeldin A: (a) Sausville, E. A.; Duncan, K. L.; Senderowicz, A.; Plowman, J.; Randazzo, P. A.; Kahn, R.; Malspeis, L.; Grever, M. R. *Cancer J. Sci. Am.* **1996**, *2*, 52–58. (b) Häcki, J.; Egger, L.; Monney, L.; Conus, S.; Rossé, T.; Fellay, I.; Borner, C. *Oncogene* **2000**, *19*, 2286–2295.

(7) Anadu, N. O.; Davisson, V. J.; Cushman, M. *J. Med. Chem.* **2006**, *49*, 3897–3905.

(8) Watari, K.; Nakamura, M.; Fukunaga, Y.; Furuno, A.; Shibata, T.; Kawahara, A.; Hosoi, F.; Kuwano, T.; Kuwano, M.; Ono, M. *Int. J. Cancer* **2012**, *131*, 310–321.

(9) (a) Evans, D. A.; Ennis, M. D.; Mathre, D. J. *J. Am. Chem. Soc.* **1982**, *104*, 1737–1739. (b) Evans, D. A.; Bartroli, J. *Tetrahedron Lett.* **1982**, *23*, 807–810.

(10) (a) Mukaiyama, T.; Kobayashi, S.; Uchiro, H.; Shiina, I. *Chem. Lett.* **1990**, 129–132. (b) Kobayashi, S.; Uchiro, H.; Fujishita, Y.; Shiina, I.; Mukaiyama, T. *J. Am. Chem. Soc.* **1991**, *113*, 4247–4252. (c) Shiina, I. In *Modern Aldol Reactions*; Mahrwald, R., Eds.; Wiley-VCH: Weinheim, 2004, pp 105–165.

(11) Reviews for IMDA reaction for the synthesis of natural products. (a) Takao, K.; Munakata, R.; Tadano, K. *Chem. Rev.* **2005**, *105*, 4779–4807. (b) Juhl, M.; Tanner, D. *Chem. Soc. Rev.* **2009**, *38*, 2983–2992.

(12) (a) Shiina, I.; Kawakita, Y. *Tetrahedron* **2004**, *60*, 4729–4733. (b) Shiina, I.; Ushiyama, H.; Yamada, Y.; Kawakita, Y.; Nakata, K. *Chem. Asian J.* **2008**, *3*, 454–461. See also (c) Shiina, I.; Kubota, M.; Oshiumi, H.; Hashizume, M. *J. Org. Chem.* **2004**, *69*, 1822–1830. (d) Shiina, I.; Umezaki, Y.; Kuroda, N.; Iizumi, T.; Nagai, S.; Katoh, T. *J. Org. Chem.* **2012**, *77*, 4885–4901.

(13) (a) Sarpong, R.; Su, J. T.; Stoltz, B. M. *J. Am. Chem. Soc.* **2003**, *125*, 13624–13625. (b) Taber, D. F.; Guo, P.; Guo, N. *J. Am. Chem. Soc.* **2010**, *132*, 11179–11182. (c) Bross, H.; Schneider, R.; Hopf, H. *Tetrahedron Lett.* **1979**, *20*, 2129–2132.

(14) DFT study of the thermal and Lewis acid catalyzed Diels–Alder reaction: (a) Goldstein, E.; Beno, B.; Houk, K. N. *J. Am. Chem. Soc.* **1996**, *118*, 6036–6043. (b) García, J. I.; Martínez-Merino, V.; Mayoral, J. A.; Salvatella, L. *J. Am. Chem. Soc.* **1998**, *120*, 2415–2420.

(15) We have succeeded in revealing the reaction mechanism of the Diels–Alder and the related reactions for the synthesis of epoxyquinols and epoxytwinol A by DFT calculations: (a) Shoji, M.; Imai, H.; Shiina, I.; Kakeya, H.; Osada, H.; Hayashi, Y. *J. Org. Chem.* **2004**, *69*, 1548–1556. (b) Shiina, I.; Uchimaru, T.; Shoji, M.; Kakeya, H.; Osada, H.; Hayashi, Y. *Org. Lett.* **2006**, *8*, 1041–1044.

(16) All calculations were performed with the program package Spartan '10 1.1.0 of Wavefunction Inc. (http://www.wavefun.com). Cartesian coordinates and energy profiles for all reported structures are included in the Supporting Information.

(17) (a) Kawai, N.; Takao, K.; Kobayashi, S. *Tetrahedron Lett.* **1999**, *40*, 4193–4196. (b) Kawai, N.; Fujibayashi, Y.; Kuwabara, S.; Takao, K.; Ijuin, Y.; Kobayashi, S. *Tetrahedron* **2000**, *56*, 6467–6478. (c) Yamakoshi, S.; Hayashi, N.; Suzuki, T.; Nakada, M. *Tetrahedron Lett.* **2009**, *50*, 5372–5375. (d) Inoue, A.; Kanematsu, M.; Yoshida, M.; Shishido, K. *Tetrahedron Lett.* **2010**, *51*, 3966–3968. (e) Gärtner, M.; Kossler, D.; Pflästerer, D.; Helmchen, G. *J. Org. Chem.* **2012**, *77*, 4491–4495.

(18) (a) Nicolaou, K. C.; Liu, J.-J.; Yang, Z.; Ueno, H.; Sorensen, E. J.; Claiborne, C. F.; Guy, R. K.; Hwang, C.-K.; Nakada, M.; Nantermet, P. G. *J. Am. Chem. Soc.* **1995**, *117*, 634–644. (b) De Koning, H.; Subramanian-Erhart, K. E. C.; Huisman, H. O. *Synth. Commun.* **1973**, *3*, 25–28. (c) Yamazaki, N.; Dokoshi, W.; Kibayashi, C. *Org. Lett.* **2001**, *3*, 193–196 .

(19) Spectroscopic data on all compounds including AMF-26 (**1**) and AMF-14 (**2**) are included in the Supporting Information.

(20) (a) Dan, S.; Tsunoda, T.; Kitahara, O.; Yanagawa, R.; Zembutsu, H.; Katagiri, T.; Yamazaki, K.; Nakamura, Y.; Yamori, T. *Cancer Res.* **2002**, *62*, 1139–1147. (b) Yamori, T. *Cancer Chemother. Pharmacol.* **2003**, *52* (Suppl 1), S74–79. (c) Yaguchi, S.; Fukui, Y.; Koshimizu, I.; Yoshimi, H.; Matsuno, T.; Gouda, H.; Hirono, S.; Yamazaki, K.; Yamori, T. *J. Natl. Cancer Inst.* **2006**, *98*, 545–556. (d) Sharma, S. V.; Haber, D. A.; Settleman, J. *Nat. Rev. Cancer* **2010**, *10*, 241–253.

(21) (a) Paull, K. D.; Shoemaker, R. H.; Hodes, L.; Monks, A.; Scudiero, D. A.; Rubinstein, L.; Plowman, J.; Boyd, M. R. J. *Natl. Cancer Inst.* **1989**, *81*, 1088–1092. (b) Monks, A.; Scudiero, D.; Skehan, P.; Shoemaker, R.; Paull, K.; Vistica, D.; Hose, C.; Langley, J.; Cronise, P.; Vaigro-Wolff, A.; Gray-Goodrich, M.; Campbell, H.; Mayo, J.; Boyd, M. *J. Natl. Cancer Inst.* **1991**, *83*, 757–766. (c) Shoemaker, R. H. *Nat. Rev. Cancer* **2006**, *6*, 813–823.

(22) In the SAR studies of brefeldin A (BFA)-related compounds, there was another example in which an acylated BFA derivative possessing cell growth inhibitory activities does not disrupt the Golgi system. See ref 7.

Biological and Pharmaceutical Bulletin Advance Publication by J-STAGE
DOI:10.1248/bpb.13-00129

Advance Publication
April 9, 2013

1 **Biol. Pharm. Bull.**

2 **Regular article**

3 **Biopharmacy**

4

5 **Search for Novel Anti-tumor Agents from Ridaifens Using JFCR39, a Panel of**

6 **Human Cancer Cell Lines**

7

8 Wen-zhi Guo[a], Yanwen Wang[b], Eri Umeda[b], Isamu Shiina[b], Shingo Dan[a], Takao Yamori[a,]

9 [c, *]

10

11 [a]*Division of Molecular pharmacology, Cancer Chemotherapy Center, Japanese*

12 *Foundation for Cancer Research, 3-8-31 Ariake, Koto-ku, Tokyo 135-8550, Japan.*

13 [b]*Department of Applied Chemistry, Faculty of Science, Tokyo University of Science,*

14 *1-3 Kagurazaka, Shinjuku-ku, Tokyo 162-860, Japan.*

15 [c]*Center for Product Evaluation, Pharmaceuticals and Medical Devices Agency, 3-3-2*

16 *Kasumigaseki, Chiyoda-ku, Tokyo 100-0013, Japan*

17

18 *Correspondence should be addressed to Takao Yamori (yamori@jfcr.or.jp).

19

Abstract

To overcome the heterogeneous nature of cancer, the search for potent anti-cancer drug candidates with new modes of action is essential. For that purpose, we prepared forty-eight Ridaifens (RIDs), a novel series of tamoxifen-derivatives. Then, we screened them, searching for novel candidates for a new class of anti-cancer drug using a panel of human cancer cell lines (JFCR39) and by a binding assay to estrogen receptor α (ERα). First, the growth inhibition of the forty-eight RIDs against JFCR39 was evaluated. Forty RIDs showed higher growth-inhibitory activity than that of tamoxifen. The structure-activity relationship (SAR) study revealed that the aminoalkoxyphenyl groups at the C-1 position and the common central ethylenic bond were important in retaining a high level of growth-inhibitory activity. Subsequently, the ERα binding activity of all the RIDs was measured by a competitive binding assay. The SAR study for ERα binding activity indicated that both the phenyl group and the ethyl group at the C-2 position in the ethylenic bond were essential. Based on the screenings, we identified RID-SB1 and RID-SB8, which demonstrated potent tumor growth inhibition but had completely lost ERα binding activity. Furthermore, the COMPARE analysis using JFCR39 suggested that RID-SB1 and RID-SB8 had different molecular modes of action compared to those of the current anti-cancer drugs including tamoxifen. These results indicate that RID-SB1 and RID-SB8 are interesting candidates for novel anticancer agents with unique modes of action.

Key words: tamoxifen-derivative;anti-cancer;JFCR39 panel;Ridaifen;novel mode of action;Drug Discovery

Introduction

Tamoxifen is an antagonist of the estrogen receptor (ER). It has been used as the first-line agent for breast cancer for more than 30 years although competitive estrogen inhibitors have been developed to treat hormonally responsive breast cancer [1-3]. The accumulative risk-benefit assessment of tamoxifen therapy has established its efficacy and safety [4-6]. Many studies of the action mode of tamoxifen have been done, which have revealed that tamoxifen is not only an estrogen blocker but also a modulator of various signaling proteins located in ER-independent biological pathways; for example protein kinase C (PKC), calmodulin, transforming growth factor β and protooncogene c-myc. Interestingly, it has been suggested that other molecules, such as caspases, mitogen-activated protein kinases (MAPK), c-jun N-terminal kinase (JNK) and p38, are involved in tamoxifen-induced apoptotic signaling [7, 8]. These reports indicate that tamoxifen potentially acts on multiple targets. Therefore, tamoxifen can be used as a lead compound to produce a new generation of anti-cancer drug with a unique mode of action, which will be used for other cancers in addition to breast cancer.

We developed a new efficient synthetic method for tamoxifen via a three-component coupling reaction [9]. Then we synthesized a series of tamoxifen derivatives, designated as Ridaifens (RIDs), expecting that they would display a variety of biological activities. As expected, we demonstrated the anti-tumor activity of three RIDs, RID-B, C, and D [10]. In this study, we further modified the structure of tamoxifen, and obtained a new series of RIDs consisting of forty-eight RIDs over three generations of modifications.

To identify anti-cancer drug candidates that have potentially unique modes of action, we had previously established a panel of 39 human cancer cell lines, designated as JFCR39, which was coupled to an anti-cancer drug activity database and a computer algorithm COMPARE [11-13]. This system provides rich and fundamental information on

the pharmacological action modes of chemicals on cancer cells. The COMPARE algorithm enabled us to identify novel drug candidates with potentially unique modes of action compared to current anticancer drugs. Moreover, it sometimes predicted the molecular targets or the modes of action of novel compounds. Indeed, by running the JFCR39 system and COMPARE, we successfully identified novel anti-cancer agents, such as a telomerase inhibitor (FJ-5002) [14], a topoisomerase I /II inhibitor (MS247) [15], a phosphatidylinositol 3-kinase inhibitor (ZSTK474) [16-18], a Golgi inhibitor (AMF-26) [19] and so on.

In the present study, we screened the forty-eight RIDs with the JFCR39 panel to identify compound that have potent growth-inhibitory activity and unique modes of action. We also evaluated the RIDs for their estrogen receptor (ER) binding activity to identify compounds which have lost ER binding activity. As a result, we found two RIDs, RID-SB1 and RID-SB8, that had potent growth-inhibitory activity against JFCR39 and had lost ERα binding activity.

Materials and methods

Chemicals

Forty-eight RIDs were synthesized over three generations of modifications. The 1st-generation of RIDs is shown in Fig. 1A. When aminoalkyl group R of the RID was R^A, R^B, R^C, R^D, R^E, R^F, R^G or R^H, each derivative was named as RID-A, RID-B, RID-C, RID-D, RID-E, RID-F, RID-G or RID-H, respectively. The 2nd-generation RIDs are based on modifications of the ethylene moiety in the 1st-generation RIDs (Fig. 1B). There are two types of the 2nd-generation RIDs, which include R^B or R^G for the aminoalkyl group R. For example, RID-SB1 has aminoalkyl group R^B as a side-chain and RID-SG1 has aminoalkyl group R^G as a side-chain. The 3rd-generation RIDs possess two identical alkyl chains ($\geq C_3$ (propyl) group) at the C-2 position, giving rise to symmetrical structures. There are three types of the 3rd-generation RIDs, bearing R^B, R^F or R^G for the aminoalkyl group R (Fig. 1C). 4-hydroxytamoxifen and tamoxifen were purchased from Sigma (St. Louis, USA). The physical properties of RID-SB1 and RID-SB8 and their ^{1}H- and ^{13}C-NMR charts were indicated in Supplemental information 1.

Cell lines

A panel of 39 human cancer cell lines, known as JFCR39, containing the following cell lines: lung cancer, NCI-H23, NCI-H226, NCI-H522, NCI-H460, A549, DMS273 and DMS 114; colorectal cancer, HCC-2998, KM-12, HT-29, HCT-15 and HCT-116, gastric cancer, MKN-1, MKN-7, MKN-28, MKN-45, MKN-74, St-4; ovarian cancer, OVCAR-3, OVCAR-4, OVCAR-5, OVCAR-8 and SK-OV-3; breast cancer, BSY-1, HBC-4, HBC-5, MDA-MB-231 and MCF-7; renal cancer, RXF-631L and ACHN; melanoma, LOX-IMVI; glioma, U251, SF-295, SF539, SF268, SNB75 and SNB78; prostate cancer, DU-145 and PC-3 , was used as described previously (1-3). All the cell

lines were cultured in RPMI 1640 medium supplemented with 5% (v/v) fetal bovine serum, penicillin (100 U/ml) and streptomycin (100 mg/ml) at 37°C in a humidified atmosphere containing 5% (v/v) CO_2.

Determination of Cell Growth Inhibition Profiles (Fingerprint)

Inhibition of cell growth was assessed by the change in total cellular protein following 48 h of treatment with a given test compound, and was measured using the sulforhodamine B (SRB) assay as described previously [20]. The 50% growth inhibition (GI_{50}) value of the drug was calculated as described previously [21]. A graphic representation (termed fingerprint) of the differential growth inhibition of each compound for the cells in the JFCR39 panel was plotted based on a calculation employing a set of GI_{50} values [22].

COMPARE Analysis

We used COMPARE analysis to assess two compounds for the similarity of their mode of action based on their fingerprints. COMPARE analysis was performed by calculating the Pearson correlation coefficient (r) between the GI_{50} mean graphs of the compounds X and Y using the following formula: $r = (\Sigma(x_i-x_m)(y_i-y_m))/(\Sigma(x_i-x_m)^2\Sigma(y_i-y_m)^2)^{1/2}$, where x_i and y_i are $LogGI_{50}$ of the two compounds, respectively, for each cell line, and x_m and y_m are the mean values of x_i and y_i, respectively ($n = 39$) [22]. The Pearson correlation coefficients were used to determine the degree of similarity. The greater the coefficient is, the higher the similarity between X and Y.

Estrogen receptor binding affinity assay

The ERα binding affinity assay was performed using recombinant ERα (Thermo, Massachusetts, USA) and the HitHunter Enzyme Fragment Complementary (EFC) Estrogen Receptor Assay kit (Discoverx Corporation, Fremont, CA) according to the manufacturer's protocol [23]. HitHunter EFC technology is based on a genetically

engineered β-galactosidase enzyme that consists of two fragments termed enzyme acceptor (EA) and enzyme donor conjugated with estradiol (ED-estradiol). Briefly, different concentrations of RIDs were added to wells containing recombinant ERα and ED-estradiol in a 384-well white plate and incubated for 1.5 h. ED-estradiol competes with RIDs in binding to ER. Any unbound ED-estradiol conjugates with EA to form an active β-galactosidase enzyme, which subsequently hydrolyzes the fluorescent substrate for luminescent detection by a microplate reader (Bio-Rad, California, USA). The excitation wavelength is 530 nm and luminosity is detected at 620 nm. The competition activity was calculated using the following formula: percent competition = (X-positive ER control)/(negative ER control-positive ER control)×100%, where X is the value of luminescent detection of RIDs. A standard curve of estradiol was run in parallel. All assays were performed in triplicates.

Results

Growth-inhibitory activities of RIDs against JFCR39

The growth-inhibitory activities of forty-eight RIDs against JFCR39 were determined by SRB assay as described in Materials and methods. Fig. 2 shows the dose response curves of the cells in the JFCR39 panel against tamoxifen and RID-SB1 as examples. The concentration at which the cell growth is inhibited by 50% represents GI_{50}. Supplemental information 2 summarizes the GI_{50} values of the forty-eight RIDs against each cancer cell line in JFCR39. The mean value of GI_{50} over all 39 cell lines (designated as MG-MID) is summarized in Table 1. The MG-MID of the RIDs ranged from 0.85 μM (RID-G) to 43.7 μM (RID-SB4). Based on the MG-MID, we found that forty of the forty-eight RIDs showed higher proliferation inhibition than tamoxifen (MG-MID = 7.41 μM).

The 1st-generation RIDs each have a pair of identical substituents (-OR) on the phenyl groups bound to the central ethylene moiety at the C-1 position (Fig. 1A). Here, the aminoalkoxy substituents were modified without changing the structures of the third phenyl group and the ethyl group at the C-2 position. The 1st-generation RIDs all showed higher anti-tumor activity than tamoxifen, except RID-D (MG-MID = 14.8 μM). These results indicate that the modifications of aminoalkyl group R with R^A~R^H except R^D enhanced the growth-inhibitory activity.

All the 2nd- and 3rd-generation RIDs have two identical aminoalkoxy substituents on both phenyl groups at the C-1 position (Fig. 1B and 1C). We selected a number of representative aminoalkyl groups for the generation of further variations of RIDs (R = R^B or R^G in the 2nd-generation; R = R^B, R^F or R^G in the 3rd-generation). The central ethylenic bond was then either removed (S4 type in Fig. 1B), or modified with two substituents at the C-2 position. The S4 type RIDs showed remarkably reduced

activities compared to tamoxifen (MG-MID = 7.41 μM) and all other RIDs. The MG-MIDs of RID-SB4 and RID-SG4 were 43.7 μM and 26.3 μM, respectively (Table 1). These results indicate that the central ethylenic bond is important for enhancing growth-inhibitory activity. On the other hand, most of the RIDs with modifications to the two C-2 substituents on the central ethylene bond did not exhibit a significant change in their growth-inhibitory activity compared to 1st -generation RIDs. The 3rd-generation RIDs have completely symmetrical structures, in which two identical alkyl chains of various lengths (C3~C6) are bound to the central ethylenic moiety. Most of them retain high levels of growth-inhibitory activity.

Each test compound was further characterized by its GI_{50} profile across JFCR39, which was designated as "fingerprint". For example, the fingerprints of tamoxifen and RID-SB1 and RID-SB8 (Supplemental information 1) were shown in Fig. 3. According to the analysis by COMPARE, the correlation coefficients between the fingerprints of tamoxifen and RID-SB1, and between tamoxifen and RID-SB8 were 0.199 and 0.318, respectively. These results suggest that RID-SB1 and RID-SB8 are different from tamoxifen with respect to their mode of action. Indeed, these two RIDs exhibited no ERα binding activity (see below).

ERα binding activities of RIDs

The ERα binding activity of the forty-eight RIDs was determined by the competitive binding of ED-Estradiol to ERα. The competitive binding curves of estradiol (positive control), tamoxifen and 4-hydroxytamoxifen are shown in Fig. 4. The y-axis indicates the percent inhibition of ED-Estradiol binding to ERα. Among the RIDs, RID-G and RID-SB1 indicated the strongest and the lowest ERα binding activity, respectively (Fig. 4).

The IC_{50} values of all of the RIDs are shown in Table 1. The relationship between

chemical structure and ERα binding activity was studied here. The 1st-generation RIDs (RID-A~H) with the various substituents on the phenyl rings at the C-1 position yielded IC_{50} values ranging from 26.6 (RID-G) to 320 nM (RID-E) (Table 1). These results indicated that the structures of substituents on the phenyl rings at the C-1 position in RIDs considerably affected the binding activity to ERα. RID-G showed ERα binding activity almost equal to tamoxifen. However, no RID compound surpassed 4-hydroxytamoxifen, an active form of tamoxifen, in ERα binding activity.

An interesting finding was observed in the ERα binding activities of the 2nd-generation RIDs. These RIDs were used to study the importance of the substituents around the C-2 position of the central ethylenic bond while retaining the two aromatic rings with identical aminoalkoxy groups at C-1. It was observed that the eight RIDs, RID-SB1, SB2, SB3 SB4, SG1, SG2, SG3 and SG4, had completely lost ERα binding activity. Structurally, these RIDs had lost either one or both of the phenyl group or the ethyl group at the C-2 position. These results clearly indicate that the phenyl and ethyl group at the C-2 position in the ethylenic bond are essential. The impact of modifications of the substituents around the ethylenic bond (RID-SB7 to SB16 and RID-SG7 to SG16) was also examined. The ERα binding activity varied significantly (23.89 ~ > 10000) depending on the modification. A trend was observed whereby the RIDs having more bulky structures around the double bond (RID-SB7 to SB12 and SG7 to SG12) displayed higher ERα binding activities (Table 1).

The 3rd-generation RIDs (RID-SG22, SG23, SG17, SG24, SB22, SB23, SB17, SB24, SF22, SF23, SF17 and SF24) (Fig.1C) and some of the 2nd-generation RIDs (RID-SG9, SG10, SB9, SB10, SF9 and SF10) (Fig.1B) have symmetrical structures. These RIDs showed lower ER binding activity in comparison to the 1st-generation RIDs (Table 1). RID-SG22, SG23, SG17, SG24, SB22, SB23, SB17, SB24, SF22, SF23, SF17 and

SF24 (3^{rd}-generation RIDs, Fig. 1C) have longer alkyl chains ($\geq C_3$ (propyl) group) than RID-SG9, SG10, SB9, SB10, SF9 and SF10 (2^{nd}-generation, Fig. 1B), and exhibited greater activities than RID-SG9, SG10, SB9, SB10, SF9 and SF10.

Two RIDs with notably high ER-independent anti-tumor activities

To evaluate the RIDs in terms of growth-inhibitory activity and ERα binding activity, a scattergram of growth inhibition (x-axis) and ERα binding activity (y-axis) for the RIDs was drawn (Fig. 5). Each spot represents one RID compound and both activities varied over a wide range. Here, we focused on two RIDs, RID-SB1 and RID-SB8 (Supporting Information 1), that had both completely lost ERα binding activity, while exhibiting the high levels of growth-inhibitory activity, suggestive that they inhibited the cell growth via an ER-independent mechanism. To confirm this point, we examined the fingerprints of the two RIDs (Fig. 3). The COMPARE analysis of RID-SB1 and RID-SB8 revealed that both of them showed a very weak correlation coefficient ($r < 0.4$) with tamoxifen (Table 2). These results suggest that both RID-SB1 and RID-SB8 have a different pharmacological mode of action to that of tamoxifen.

COMPARE analysis of RID-SB1 and RID-SB8

We previously established the JFCR39 drug database and COMPARE analysis and demonstrated that this system is a powerful tool for use in identifying the molecular targets or pharmacological modes of action of novel compounds [11-13]. The JFCR 39 drug database integrates the fingerprints of reference compounds including 87 standard drugs currently used in clinic and more than 1100 inhibitors of various enzymes and biological pathway. To investigate the possible modes of action of RID-SB1 and RID-SB8, we carried out the COMPARE analysis. The two RIDs did not correlate with any currently used anti-cancer drugs ($r < 0.4$). Table 2 summarized the top three reference compounds, which were extracted from the database due to the similarity of

their fingerprint profiles to RID-SB1 or RID-SB8. It was indicated that RID-SB1 was most similar to NVP-AEW541 (IGF-1R inhibitor), Bortezomib (proteasome inhibitor) and RDEA119 (MEK inhibitor). RID-SB8 was most similar to PB28 dihydrochloride (sigma-2 receptor agonist), MEK inhibitor I (MEK inhibitor) and Raf 1 Kinase Inhibitor I (Raf 1 kinase inhibitor). Although the correlation coefficients were not high enough, the targets of these reference compounds could be the targets of RID-SB1 or RID-SB8.